The Chandra Source Catalog: X–ray Aperture Photometry

Vinay L. Kashyap[1], F.A. Primini[1], K.J. Glotfelty[1], C.S. Anderson[1], N.R. Bonaventura[1], J.C. Chen[1], J.E. Davis[2], S.M. Doe[1], I.N. Evans[1], J.D. Evans[1], G. Fabbiano[1], E. Galle[1], D.G. Gibbs[1], J.D. Grier[1], R. Hain[1], D.M. Hall[1], P.N. Harbo[1], X. He[1], J.C. Houck[2], M. Karovska[1], J. Lauer[1], M.L. McCollough[1], J.C. McDowell[1], J.B. Miller[1], A.W. Mitschang[1], D.L. Morgan[1], J.S. Nichols[1], M.A. Nowak[2], D.A. Plummer[1], B.L. Refsdal[1], A.H. Rots[1], A.L. Siemiginowska[1], B.A. Sundheim[1], M.S. Tibbetts[1], D.W. Van Stone[1], S.L. Winkelman[1], P. Zografou[1]

[1]**Smithsonian Astrophysical Observatory; [2]MIT Kavli Institute for Astrophysics and Space Research**

472.09 : AAS 2009 : Long Beach, CA

The Chandra Source Catalog (CSC) represents a reanalysis of the entire ACIS and HRC imaging observations over the 9-year Chandra mission. We describe here the method by which fluxes are measured for detected sources. Source detection is carried out on a uniform basis, using the CIAO tool wavdetect. Source fluxes are estimated post-facto using a Bayesian method that accounts for background, spatial resolution effects, and contamination from nearby sources. We use γ-function prior distributions, which could be either non-informative, or in case there exist previous observations of the same source, strongly informative. The current implementation is however limited to non-informative priors. The resulting posterior probability density functions allow us to report the flux and a robust credible range on it. We first set up the problem (**§1**) and describe the classical solution that usually applies in the high counts regime (**§2**). We then develop the general Bayesian solution (**§3**). Some advantages and disadvantages of this method are discussed in **§4**. Example output is shown below in **Figure 3**.

1. NOTATION

- We suppose that n_S counts are present in the source aperture (**Figure 1**) and n_B counts in an annular aperture around it.
- If A_S and A_B are the areas of these apertures, the fraction of source counts expected in them due to the finite extent of the PSF is

$$f = \int_{A_S} PSF(x,y)\, \varepsilon_S\, dx\, dy \quad ; \quad g = \int_{A_B} PSF(x,y)\, \varepsilon_B\, dx\, dy\,, \qquad (1)$$

  where ε represents an efficiency factor representing the average effective area or the exposure times for the relevant regions. Note that f and g can thus include a counts-to-flux conversion factor without loss of generality. In practice, we use $\varepsilon = 1$.
- Typically, model parameters are represented with Greek letters and data quantities are represented by Roman letters. Thus, the intrinsic source intensities are represented as θ_S and θ_B respectively, and the observed data are realizations of the intrinsic intensity,

$$n_S \sim \mathrm{Pois}(\lambda_S) \quad ; \quad n_B \sim \mathrm{Pois}(\lambda_B)\,, \qquad (2a)$$

  with

$$\lambda_S \equiv f\cdot\theta_S + \theta_B \quad ; \quad \lambda_B \equiv g\cdot\theta_S + r\cdot\theta_B\,, \qquad (2b)$$

  and $r = A_B/A_S$.
- In Bayesian analysis, it is customary to denote the probability density function of variable x, conditional on another variable y, as $p(x|y)$. The probability of a hypothesis H, generally a single number, is denoted as $p(H)$. A parameter θ that takes a variety of values can be represented as a distribution, $p(\theta|data)$. Here, we compute

$$p(\theta_S|n_S,n_B,f,g,r) \equiv \int d\theta_B\; p(\theta_S,\theta_B|n_S,n_B,f,g,r)\,. \qquad (3)$$

2. CLASSICAL CASE

- The standard practice in X-ray aperture photometry has been to ignore the Poisson nature of the problem (**Equation 2**) and to compute the maximum likelihood estimates of the source and background intensities $\hat{\theta}_S$ and $\hat{\theta}_B$ by solving the algebraic equations

$$n_S = f\cdot\hat{\theta}_S + \hat{\theta}_B \quad ; \quad n_B = g\cdot\hat{\theta}_S + r\cdot\hat{\theta}_B\,, \qquad (4)$$

- Solving **Equation 4** for $\hat{\theta}_S$ and $\hat{\theta}_B$,

$$\hat{\theta}_S = \frac{r n_S - n_B}{r f - g} \quad ; \quad \hat{\theta}_B = \frac{f n_B - g n_B}{r f - g}\,, \qquad (5a)$$

  with errors propagated under a Gaussian assumption,

$$\sigma_S^2 = \frac{r^2 n_S + n_B}{(r f - g)^2} \quad ; \quad \sigma_B^2 = \frac{f^2 n_B + g^2 n_B}{(r f - g)^2}\,. \qquad (5b)$$

- The classical case is a useful approximation in the high counts regime, when $n_S, n_B, n_S - n_B \gg 1$ and when $f \approx 1, g \approx 0$. However, this condition is usually not met for the majority of X-ray sources, and the estimates and uncertainties derived thus become unreliable (**Figure 2**).

3. BAYESIAN ANALYSIS

- A number of Bayesian calculations have previously estimated the probability density of source intensities given a background measurement (e.g., Loredo 1990, Loredo 1992, van Dyk et al. 2002, Kashyap et al. 2008). However, these calculations, of $p(\lambda_S|n_S,n_B)$ (see **Equation 2**), do not account for the contamination of the counts in the background region A_B by source counts that spill over due to the Point Spread Function (Primini 2004).
- The basis of our calculation is Bayes' Theorem, which allows inclusion of both likelihood and prior information in the estimation of the intensities in the measurement areas. In general, we have

$$p(\lambda_S,\lambda_B|\mathrm{Data}) = \frac{p(\lambda_S,\lambda_B)\,p(\mathrm{Data}|\lambda_S,\lambda_B)}{p(\mathrm{Data})}\,, \qquad (6)$$

  where the denominator represents a normalizing constant, and the first term in the numerator is the prior and the second term, the likelihood.
- We transform variables from $\{\lambda_S,\lambda_B\} \to \{\theta_S,\theta_B\}$ (**Equation 2b**),

$$\begin{aligned} p(\lambda_S,\lambda_B|n_S,n_B,g,f,r)\, d\lambda_S d\lambda_B &= p(\theta_S,\theta_B|n_S,n_B,g,f,r)\left|\frac{\partial(\lambda_S,\lambda_B)}{\partial(\theta_S,\theta_B)}\right| d\theta_S d\theta_B \\ &= p(\theta_S,\theta_B|n_S,n_B,g,f,r)(rf-g)\,d\theta_S d\theta_B\,. \qquad (7) \end{aligned}$$

- In general, we use γ-function priors for both λ_S and λ_B,

$$\begin{aligned} p(\lambda_S) &= \frac{\beta_S^{\alpha_S}\lambda_S^{\alpha_S-1}\, e^{-\beta_S\lambda_S}}{\Gamma(\alpha_S)}\,, \qquad (8a) \\ p(\lambda_B) &= \frac{\beta_B^{\alpha_B}\lambda_B^{\alpha_B-1}\, e^{-\beta_B\lambda_B}}{\Gamma(\alpha_B)}\,, \qquad (8b) \end{aligned}$$

  with the parameters set to a form that is non-informative, $\alpha_S = \alpha_B = 1$ and $\beta_S = \beta_B = 0$.
- The likelihood is taken to be Poisson.
- After considerable algebra, we find

$$\begin{aligned} p(\theta_S|n_S,n_B,f,g,r) = {} & d\theta_S\,(rf-g)\frac{1}{\Gamma(n_S+1)\Gamma(n_B+1)} \times \\ & \sum_{k=0}^{n_S}\sum_{j=0}^{n_B}\Big(f^k\, g^j\, r^{n_B-j}\, \theta_S^{k+j}\, e^{-\theta_S(f+g)} \times \\ & \frac{\Gamma(n_S+1)\Gamma(n_B+1)\Gamma(n_S+n_B-k-j+1)}{\Gamma(k+1)\Gamma(n_S-k+1)\Gamma(j+1)\Gamma(n_B-j+1)(1+r)^{n_S+n_B-k-j+1}}\Big)\,. \qquad (9) \end{aligned}$$

4 Advantages & Disadvantages

+ Includes effect of the PSF spilling over into the putative background region.
+ Produces correct estimates and uncertainty intervals even in low counts regime. Uncertainties are reported as an equal-tailed 68% interval. Because the full probability density function of θ_S can be calculated, highest-posterior-density or Gaussian-equivalent intervals can also be computed.
+ Overlapping sources can be dealt with using non-elliptical apertures that (mostly) exclude the contributions due to the contaminating source.
+ While current implementation assumes non-informative priors, it is straightforward to include prior information in the form of a previous measurement. Multiple observations of the same object with different instruments and telescopes can be daisy-chained to reduce error bars.

– Conceptually simple, but computationally complex.

– Numerical estimation can be costly in the high counts regime. We switch to the classical case (§2) for $(n_S + n_B) > 50$.

– Lack of a simple algebraic solution means the solution remains unintuitive.

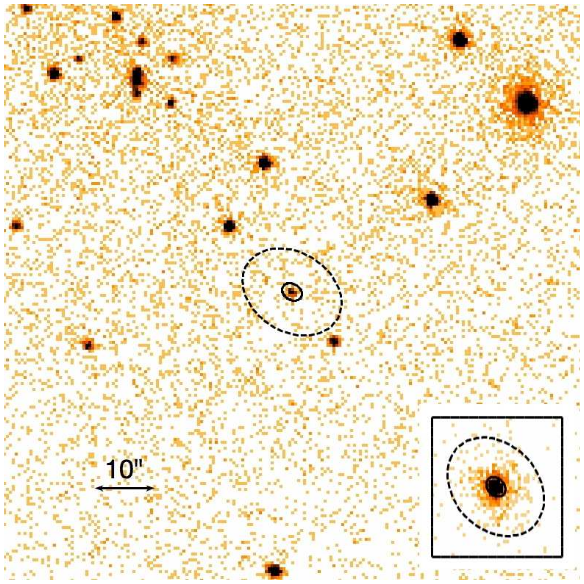

Figure 1: A typical *Chandra* image, showing an aperture centered on the source and an annular aperture around it that is dominated by the background. The inset figure displays a ChaRT simulation of a point source appropriate for this location, with the same regions overlaid. Note that a considerable fraction of the source counts fall into the putative background aperture. Accounting for this (via f and g, see **Equation 1**) is an important factor in the analysis.

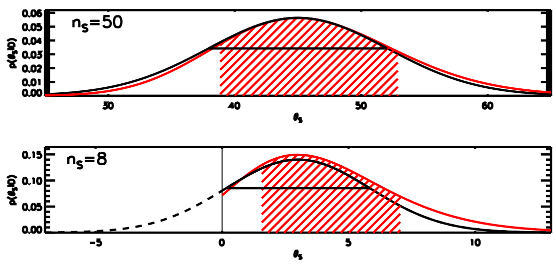

Figure 2: Comparison of classical approximation with Poisson. The Bayesian posterior density function $p(\theta_S|\mathrm{Data})$ (**Equation 9**) is shown as the red curve, compared with the Gaussian density function in black. The former is defined only over the non-negative number line, whereas the latter is not so restricted. The shaded regions represent the 68% equal-tailed interval, and the solid horizontal line represents the classical $\pm 1\sigma$ interval ((**Equation 5**). The upper plot is for the high counts case ($n_S = 50$) and the lower plot is for the low counts case ($n_S = 8$). In both cases the same background ($n_B = 200$), areas ($r = 40$), and PSF fractions ($f = 1, g = 0$) were used. Notice that the Gaussian approximation is reasonable for high counts, but is invalid in the low counts regime.

REFERENCES

– Kashyap, V., van Dyk, D., Connors, A., Freeman, P., Siemiginowska, A., Zezas, A., & the SAMSI-SaFeDe Collaboration, 2008, AAS-HEAD #10, 03.02
`http://hea-www.harvard.edu/AstroStat/HEAD2008/#0302`

– Loredo, T.J., 1990, in "Maximum Entropy and Bayesian Methods", ed. P.F. Fougere (Dordrecht:Kluwer), 81

– Loredo, T.J., 1992, in "Statistical Challenges in Modern Astronomy", eds. E.D. Feigelson and G.J. Babu, Springer-Verlag, New York, pp. 275-297

– Primini, F.A., 2004, CSC Memo,
`http://cxc.cfa.harvard.edu/csc/memos/files/Primini_significance.pdf`

– van Dyk, D.A., Connors, A., Kashyap, V.L., & Siemiginowska, A., 2001, ApJ, 548, 224

Query Results Log Help

Back to Query — 10 rows loaded at 2008-12-29T09:00:29

name	o.livetime	o.area_aper90	o.area_aper90bkg	o.cnts_aper90_b	o.cnts_aper90bkg_b	o.src_cnts_aper90_b	o.src_rate_aper90_b	o.src_rate_aper90_hilim_b	o.src_rate_aper90_lolim_b
CXO J000000.1+623123	49332.1	103.36	2737.3	17	130	14.163	0.00028709	0.00037951	0.00019395
CXO J000001.4+623148	49332.1	115.47	4015.4	40	204	38.294	0.00077624	0.00091647	0.00063460
CXO J000002.3-552443	53210.8	93.437	4033.3	43	842	29.946	0.00056279	0.00070264	0.00042299
CXO J000002.9+623155	49332.1	129.75	4958.2	24	252	20.150	0.00040846	0.00051923	0.00029797
CXO J000004.4-552604	53210.8	94.405	6224.0	148	1310	141.04	0.0026506	0.0029003	0.0024035
CXO J000004.4-552604	19947.9	94.647	4244.4	42	357	40.142	0.0020123	0.0023732	0.0016478
CXO J000005.3+623029	49332.1	104.09	5906.9	24	280	22.620	0.00045853	0.00056935	0.00034849
CXO J000005.8+622138	49328.9	176.47	2427.2	28	148	21.029	0.00042629	0.00054772	0.00030497
CXO J000006.7+622621	49328.9	73.103	2609.5	16	106	14.084	0.00028550	0.00037257	0.00019771
CXO J000007.8-552156	53210.8	183.49	4786.1	147	2263	80.172	0.0015067	0.0017678	0.0012482

Figure 3: A display of the CSC viewer tool showing exemplar results of the X-ray aperture photometry. The quantities listed for each source ID are:
– exposure time τ [sec],
– source cell area [arcsec^2],
– background cell area [arcsec^2],
– n_S [ct],
– n_B [ct],
– θ_S [ct],
– θ_S/τ [ct s^{-1}],
– and the 68% equal-tail uncertainty interval on θ_S/τ [ct s^{-1}], based on the 84th- and 16th-percentile levels of the posterior probability density function $p(\theta_S/\tau|\mathrm{Data})$
The PSF fractions are $f = 0.9$ and $g = 0.1$ in all cases.

vkashyap@cfa.harvard.edu

This work was supported by CXC NASA contracts NAS8–39073 (VK) and NAS8–03060 (CSC)